International Journal of Nanomedicine

Dovepress
open access to scientific and medical research

Open Access Full Text Article

ORIGINAL RESEARCH

A Three-Dimensional Printed Polycaprolactone Scaffold Combined with Co-Axially Electrospun Vancomycin/Ceftazidime/Bone Morphological Protein-2 Sheath-Core Nanofibers for the Repair of Segmental Bone Defects During the Masquelet Procedure

This article was published in the following Dove Press journal:
International Journal of Nanomedicine

Yi-Hsun Yu[1,2]
Demei Lee[2]
Yung-Heng Hsu[1,2]
Ying-Chao Chou[1,2]
Steve WN Ueng[1]
Che-Kang Chen[2]
Shih-Jung Liu[1,2]

[1]Department of Orthopedic Surgery, Musculoskeletal Research Center, Chang Gung Memorial Hospital, Taoyuan, Taiwan; [2]Department of Mechanical Engineering, Chang Gung University, Taoyuan, Taiwan

Introduction: Masquelet proposed a new solution for the healing of segmental bone defects, thus minimizing the disadvantages associated with traditional bone grafting. However, a major factor leading to the failure of this technique pertains to be the residual infection. Accordingly, we developed an antibiotic- and osteo-inductive agent-loaded composite scaffold to solve this problem.

Methods: A mesh-like polycaprolactone scaffold was prepared using a lab-exploited solution-type three-dimensional printer, and hybrid sheath-core structured poly(lactic-co-glycolic-acid) nanofibers were fabricated using co-axial electrospinning technology. Vancomycin, ceftazidime, and bone morphological protein (BMP)-2 were employed. The in vitro and in vivo (rabbit fracture model) release patterns of applied agents from the composite scaffold were investigated.

Results: The results revealed that the drug-eluting composite scaffold enabled the sustainable release of the medications for at least 30 days in vitro. Animal tests demonstrated that a high concentration of medications was maintained. Abundant growth factors were induced within the bioactive membrane stimulated by the applied scaffold. Finally, satisfactory bone healing potential was observed on radiological examination and biomechanical evaluation.

Discussion: The developed composite scaffold may facilitate bone healing by inducing bioactive membrane formation and yielding high concentrations of antibiotics and BMP-2 during the Masquelet procedure.

Keywords: Masquelet procedure, composite scaffold, three-dimensional printing, co-axial electrospinning

Introduction

Masquelet proposed a new solution for the healing of segmental bone defects, called the induced membrane technique. The clinical benefits of this technique have been reported, including reducing the need for tying with an external fixator for a long time (distraction osteogenesis)[1–3] and decreasing functional disability due to strut bone graft transplantation surgery (free vascularized fibula bone graft).[4,5] However, a major factor leading to the failure of bone union after membrane induction is a residual infection in segmental

Correspondence: Shih-Jung Liu
Biomaterials Lab, Department of Mechanical Engineering, Chang Gung University, No. 259 Wen-Hwa 1st Road, Guishan District, Taoyuan 333, Taiwan
Tel +886 3 211 8166
Fax +886 3 211 8558
Email shihjung@mail.cgu.edu.tw

submit your manuscript | www.dovepress.com
DovePress
http://doi.org/10.2147/IJN.S238478

bone defects.[6] Several studies have proposed using antibiotic-loaded polymethmethylacrylate (PMMA) spacers for the eradication of infection; however, the results of the treatment varied among different studies.[7,8]

Resorbable polymers have been used in medical applications since the 1930s. Currently, these materials are commonly used as sutures for wound repair, internal fixators for fracture fixation,[9] media for drug delivery,[10,11] and scaffolds for tissue engineering.[12] Among these applications, the clinical uses of resorbable polymers in detonated drug delivery and tissue engineering have been widely applied. The main advantage of using resorbable polymers as a carrier in drug delivery is related to their capacity for controlled drug release targeted to specific medical purposes. Once the carried drug has been eluted completely, the carrier made from the resorbable polymer is hydrolyzed and dissolved. Furthermore, the system of drug delivery can simultaneously incorporate two or more drugs with dissimilar medical utilities in one polymer or in hybrid polymer composites, further expanding the potential applications of this approach.

Poly(lactic-co-glycolic-acid) (PLGA) and polycaprolactone (PCL) are the two most common resorbable polymers applied in the orthopedic field. PLGA has the advantages of being nontoxic to tissues[13] and a good carrier for drug release,[14] causing minimal inflammatory response during degradation[15–17] and producing biocompatible end products.[18] Several studies have shown that PLGA is a good carrier for bone morphogenetic protein (BMP), which enhances bone healing.[11,19] PCL shows the same advantages as PLGA but has a longer degradation time. Thus, PCL can serve as a good reservoir for preserving bone grafts until bone healing occurs.[20]

In a previous study in our laboratory, we demonstrated the effectiveness of inducing a bioactive membrane from the modified Masquelet procedure by replacing the PMMA spacer with resorbable PLGA nanofibers.[21] In the current study, we further explored the applications of drug-loaded nanofibers in the context of infection during the Masquelet process. We hypothesized that implantation of antibiotic- and osteo-inductive agent-loaded composite scaffolds in segmental bone defects could permit the continuous release of the agents into adjacent tissues to promote bone defect healing.

Materials and Methods

Materials

Commercially available PCL (molecular weight: 70,000–90,000 Da) and PLGA (molecular weight: 24,000–38,000 Da; LA:GA = 50:50, Resomer RG 503) were acquired from Sigma-Aldrich (St. Louis, MO, USA). The antibiotics (vancomycin hydrochloride and ceftazidime hydrate), solvents for the polymers (dichloromethane [DCM] and hexafluoro-2-propanol [HFIP]), and powdered recombinant human BMP-2 (rhBMP-2) were also purchased from Sigma-Aldrich.

Three-Dimensional (3D) Printing of PCL Scaffolds

The PCL mesh-like scaffold was prepared using a lab-exploited solution-type 3D printer manufactured specifically for this study. The printer consisted of a solution-type plunger-actuated feeding system, stepper motors and motion components, a power supply unit, a print bed, and a user interface with connectivity. Before printing, 2.5 mg PCL was first dissolved in 3.75 mL DCM. The solution was then loaded into a solution-type feeder (a syringe) equipped with a plastic nozzle with an outlet diameter of 0.18 mm for printing. During printing, the feeder was actuated by a servo motor, and the PCL solution was extruded onto the print bed. After the evaporation of DCM, the PCL filament (approximately 0.2 mm in diameter) was deposited onto the printer bed surface layer by layer. Mesh-like PCL scaffolds were thus obtained. Figure 1A shows a photograph of the printed PCL meshes.

Fabrication of Vancomycin/Ceftazidime and BMP-2 Nanofibrous Membranes

The drug-eluting nanofibrous membranes consisted of two layers, namely an electrospun PLGA/vancomycin/ceftazidime layer and a co-axially spun PLGA/BMP-2 layer. To prepare the first layer, 250 mg PLGA, 20 mg vancomycin, and 20 mg ceftazidime were mixed with 1 mL HFIP for 12 h and then electrospun into nonwoven nanofibrous membranes via a syringe with a needle measuring 0.42 mm in diameter. The delivery rate of the solution was 1.2 mL/h. This was followed by co-axial electrospinning of sheath-core-structured PLGA/BMP-2 nanofibers. A special co-axial device that delivers two polymer solutions simultaneously was employed.[14] Then, 100 μg rhBMP-2 and 1 mg bovine serum albumin were mixed with 1 mL phosphate-buffered solution. The PLGA and rhBMP-2 solutions were then loaded into two separate syringes with needles for co-axial electrospinning at room temperature. During spinning, the

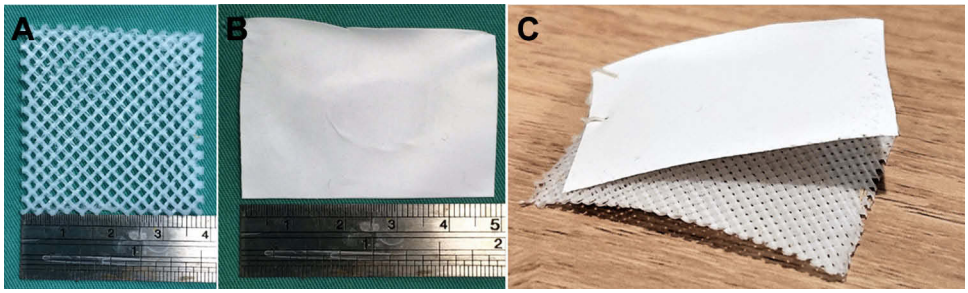

Figure 1 Photographs of (**A**) PLC mesh, (**B**) PLGA composite nanofibers, and (**C**) PLGA-PCL composites.

solutions were delivered by two independently controlled pumps with different volumetric flow rates: 0.9 mL/h for the sheath PLGA solution and 0.3 mL/h for the core rhBMP-2 solution. The solution in the syringe was set at a positive potential of 15 kV, and the travel distance for the ejected solution from the needle tip to the collection plate (ground electrode) for the fibers was 15 cm. The collection plate was mounted on a reciprocal shaker (Major Science, CA, USA) in order to obtain nanofibrous membranes of uniform thickness. The thickness of the two-layered hybrid nanofibrous membrane thus obtained was approximately 0.12 mm (Figure 1B).

Bioactivity of the Vancomycin/Ceftazidime PLGA Membrane

The bioactivities of eluted released antibiotics were determined by a disk diffusion method. The target bacteria and method of determination of bioactivity were described in our previous work.[11]

Scanning Electron Microscopy (SEM)

The morphology of electrospun nanofibers was observed on a field-emission scanning electron microscope (model JSM-7500F; JEOL, Japan) after gold coating. The average diameter and diameter distribution were obtained by analyzing SEM images using commercial ImageJ software (National Institutes of Health, Bethesda, MD, USA).

The densities of the electrospun nanofibers were calculated by dividing their masses by their volumes. The apparent porosity of the nanofibers was calculated using the following equation

$$\text{Pore}(\%) = \left\{ 1 - \frac{\rho_{\text{membrane}}}{\rho_{\text{polymer}}} \right\} \quad (1)$$

where ρ_{membrane} and ρ_{polymer} represent the densities of the nanofibers and the polymer, respectively.

Transmission Electron Microscopy (TEM)

Co-axially spun nanofibers were laid upon a copper network (Pelco Products Inc., OK, USA) and examined by field-emission TEM (JEM-2000EXII; JEOL, Tokyo, Japan).

Contact Angle Measurement of Nanofibers

A water contact angle analyzer (First Ten Angstroms, Portsmouth, VA, USA) was employed. Specimens (1 cm × 1 cm) were excised from electrospun nanofibrous membranes and placed on the testing plate, after which distilled water was dropped onto the membrane surfaces. The contact angles of virgin PLGA nanofibers, sheath-core PLGA/BMP-2 nanofibers, and PLGA/vancomycin/ceftazidime nanofibers were characterized using a camera.

In vitro Elution Profiles of Electrospun and Co-Axially Electrospun Nanofibers

Standard elution curves of antibiotics and osteo-inductive agent were generated prior to the animal study. The vancomycin/ceftazidime PLGA nanofibers were examined in an environment containing 1 mL phosphate-buffered solution in the test tube under a constant temperature (37°C). The studied solution was collected every 24 hrs for 30 days. The collected solution was then characterized by high-performance liquid chromatography (HPLC) to establish standard drug-elution curves. HPLC analyses were conducted on a Hitachi L-2200 Multisolvent Delivery System. A SYMMETRY C8 column (3.9 cm × 150 mm) was used to characterize vancomycin and ceftazidime (Waters, Milford, MA, USA). The mobile phase containing 0.01 mol heptanesulfonic acid (Fisher Scientific, Loughborough, UK) and acetonitrile (Mallinckrodt, St. Louis, MO, USA; 85/15, v/v) was employed to separate vancomycin. The absorbance wavelength was set at 280 nm, and the flow rate was 1.4 mL/min. The mobile phase used for ceftazidime contained methanol and 5 mM phosphate buffer (pH 7.5;

Sigma-Aldrich; 10/90, v/v). The absorbance was monitored at 254 nm with a flow rate of 0.6 mL/min. All experiments were performed in triplicate (n = 3).

The BMP-2 elution profile was quantified using a commercialized enzyme-linked immunosorbent assay (ELISA) kit (R&D Systems, Inc., Minneapolis, MN, USA) according to the manufacturer's instructions. Briefly, BMP-2 quantification was performed in 96-well plates by measuring the optical density at 450 nm after the addition of a colorimetric substrate solution. A standard elution curve for the BMP-2 concentration was thus generated.

In vivo Animal Model

All animal procedures were performed after obtaining approval from the Animal Care Center of Chang Gung University (approval no. CGU106-058), and the postoperative care of animals for wound sterilization and pain was performed using standard approaches according to the regulations for animal care established by Chang Gung University. A critical bone defect model was designed using the femurs of New Zealand rabbits in order to test our hypothesis. Fifteen healthy adult rabbits with different but controlled weights between 2000 and 2500 g were used in this experiment. Prior to the surgical procedure, a high-flow oxygen supplement was first given to the experimental rabbits for 10 min to help establish anesthesia safety. Inhalation anesthesia with isoflurane was then used for induction of anesthesia and throughout the entire surgical procedure. The rabbits were placed in the decubitus position with the right-side femur positioned up. Using standard sterile procedures, an 8-cm surgical incision was made along the femur. Next, a sharp dissection between muscle layers was performed to expose the target femur. During the surgical approach, small vessels were ligated surgically without the use of an electrocauterization device. After the femur was identified, a critical size bone defect (10 mm in length) was created using an osteotome on the middle diaphysis. An intramedullary Kirchner wire with a diameter of 1.8 mm was inserted in a retrograde fashion, and two 2.0-mm stainless compressive screws were applied on each side of a 10-hole stainless plate to complete the osteosynthesis procedure for the femur.

Following the femoral osteotomy fixation procedure, we divided the studied rabbits randomly into three groups: 3D-printed PCL mesh group (PCL group); 3D-printed PCL mesh with electrospun vancomycin/ceftazidime PLGA nanofibers group (PCL-PLGA/antibiotic group), and 3D-printed PCL mesh with electrospun and co-axially electrospun vancomycin/ceftazidime/BMP-2 PLGA nanofibers group (PCL-PLGA/antibiotic/BMP-2 group). All femoral defects were first filled with an artificial bone substitute (Foramic Bone Substitute Granules, Maxigen Biotech Inc., Taiwan). In the PCL group, the fabricated 3D PCL mesh was wrapped circumferentially to cover all of the bone defect. In the other two groups (PCL-PLGA/antibiotic group and PCL-PLGA /antibiotic/BMP-2 group), the mesh and the nanofibrous membranes composites (Figure 1C) were wrapped circumferentially to cover all of the bone defect. The surgical wound was then closed layer by layer with absorbable sutures after completing all surgical procedures.

In vivo Drug Release Profiles

Examination of drug-eluting efficacy was performed by measuring systemic drug concentrations in the blood and local drug concentrations within tissues, except for in the PCL group. The procedures for systemic and local tissue sampling were performed on days 1, 7, 14, 28, and 42 after the operation. Blood samples (0.5 mL) were obtained from the arterial blood of the rabbit's ear to detect the systemic concentration of antibiotics. Tissue samples were obtained from the muscle of the vastus lateralis, which was closest to the applied resorbable scaffolds, through the same surgical wound. Each sample weighed and adjusted to 20–30 mg. During the sampling procedure, the sterile procedure and animal care were exactly the same as that in the initial surgery, as described above. The samples were then processed and analyzed by HPLC analysis and ELISA for the detection of local concentrations of applied antibiotics and growth factors, respectively.

Histologic Evaluation of the Specimen

The tissue samples obtained from the investigated animals were preserved in 10% phosphate-buffered formalin and sliced into 2-mm-thick fragments, which were processed and embedded in paraffin. Tissue sections (4 μm) were obtained using a microtome (Sakura Finetek, Tokyo, Japan) for evaluation. Additionally, the obtained samples were blotted with hematoxylin and eosin and observed under a microscope with magnification up to 400x.

Immunohistochemical (IHC) Evaluation of the Specimen

Standard IHC staining was performed on 4-μm-thick paraffin sections of the membrane tissue for the expression of BMP-2, vascular endothelial growth factor (VEGF), von Willebrand

factor (vWF), transforming growth factor (TGF)-β, and interleukin (IL)-6. After deparaffinization, heat-induced epitope retrieval was performed (95°C/30 min) in citrate buffer (pH = 6.0). Commercial antibodies were adapted for IHC analysis; these included anti-BMP-2 (polyclonal, 1:200; cat. no. A0231; ABclonal, MA, USA); anti-VEGF (polyclonal, 1:200; cat. no. A0280; ABclonal); anti-vWF (vWF Picoband antibody, 1:200; cat. no. PB9062; Boster Biological Technology, Pleasanton CA, USA); anti-TGF-β (polyclonal, 1:200; cat. no. A2561; ABclonal); and anti-IL-6 (polyclonal, 1:200; cat. no. A0286; ABclonal). Endogenous peroxidase was quenched in a 0.3% hydrogen peroxide and 50% methanol solution for 10 min, followed by rinsing in phosphate-buffered saline (PBS). TAHC-04D (BioTnA, Taiwan) was employed as the signal detecting system.

Radiographic Examination

Image evaluation was conducted by radiographic examinations on days 7, 28, and 56 after the surgery in order to document fracture healing. The anesthesia procedure for the X-ray examination was the same as that described above.

Mechanical Properties: Torsional Test

After examination of femur specimens, the specimens were sent for mechanical testing. The femur has the weakest bearing ability under torsional force, compared with compressive and tensile forces. Therefore, in this study, we employed a torsional mechanical test to compare mechanical forces among healthy and test femurs. Before the mechanical test, the muscular tissue and implanted metal plate were removed gently in order to preserve the integrity of the specimen. Both ends of each femoral specimen were stabilized by embedding in cylindrical epoxy blocks (radius = 1.5 cm, thickness = 1.3 cm) before testing on a torsional testing machine (Gotech Testing Machines, Inc., Taichung, Taiwan) for the rotational torque and toughness assessments. The rotational speed of the loading head was set at 1.0 rpm. Data from the mechanical torsional test were analyzed using SPSS version 18.0 statistical software (SPSS Inc., Chicago, IL, USA).

Results

Characterization of Fabricated Scaffolds

All PLGA nanofibrous specimens (PLGA, vancomycin/ceftazidime PLGA, and BMP-2 PLGA nanofibers) were examined by field-emission SEM. Figure 2 shows the SEM images and fiber diameter distributions of the prepared nanofibers. The average diameters were 1.04 ± 0.38 μm, 1.58 ± 0.54 μm, and 111.68 ± 45.11 nm for pure PLGA nanofibers, PLGA/BMP-2 nanofibers, and PLGA/vancomycin/ceftazidime nanofibers, respectively. The average porosities of the specimens were 61.12%, 73.68%, and 54.23%, respectively. Additionally, Figure 3 shows TEM images of electrospun nanofibers, demonstrating the sheath-core structure of the fibers.

The water contact angles for all PLGA nanofibrous specimens were also examined (Figure 4). The measured contact angles for pure PLGA nanofibers, PLGA/BMP-2 nanofibers, and PLGA/vancomycin/ceftazidime nanofibers were 126.24 ± 10.26°, 120.00 ± 8.67°, and 69.2.33 ± 5.14°, respectively. The hydrophilicity of the electrospun nanofibers was substantially improved with the addition of water-soluble antibiotics.

In vitro Elution Profiles

The drug-eluting profiles of the electrospun PLGA/vancomycin/ceftazidime nanofibrous membranes are shown in Figure 5. Peak elution of vancomycin was observed on the first day (approximately 25–30%), followed by a second peak on day 6 (Figure 5A). After the second peak, there was a constant elution trend until day 30. Regarding the elution profile of ceftazidime, although greater daily variation in the elution concentration was observed before day 7, the obtained elution trend was similar to that of vancomycin. During the in vitro test, the PLGA nanofibrous membranes were not noticeable after being eluted in PBS for more than 2 months.

The accumulated drug-elution profiles of vancomycin and ceftazidime were also examined (Figure 5B). Both antibiotics showed similar trends, and the accumulated drug-elution percentages reached near 90% (vancomycin: 86.4%, ceftazidime: 83.9%) on day 30.

The daily elution profile of BMP-2 PLGA nanofibers is shown in Figure 5C. Continuous, regular elution of BMP-2 from PLGA nanofibers was observed (range: 56.9–65.6 pg/mL) for up to 25 days, except for one sample on day 13. The elution curve of BMP-2 PLGA nanofibers showed nearly total release at the end of the examination (Figure 5D).

In vivo Drug Release Profiles

Vancomycin/Ceftazidime and BMP-2 Concentrations in Local Tissue

The concentrations of vancomycin of ceftazidime from local muscular tissue are shown in Figure 5E. The in vivo release of the two antibiotics from PLGA nanofibers showed a similar

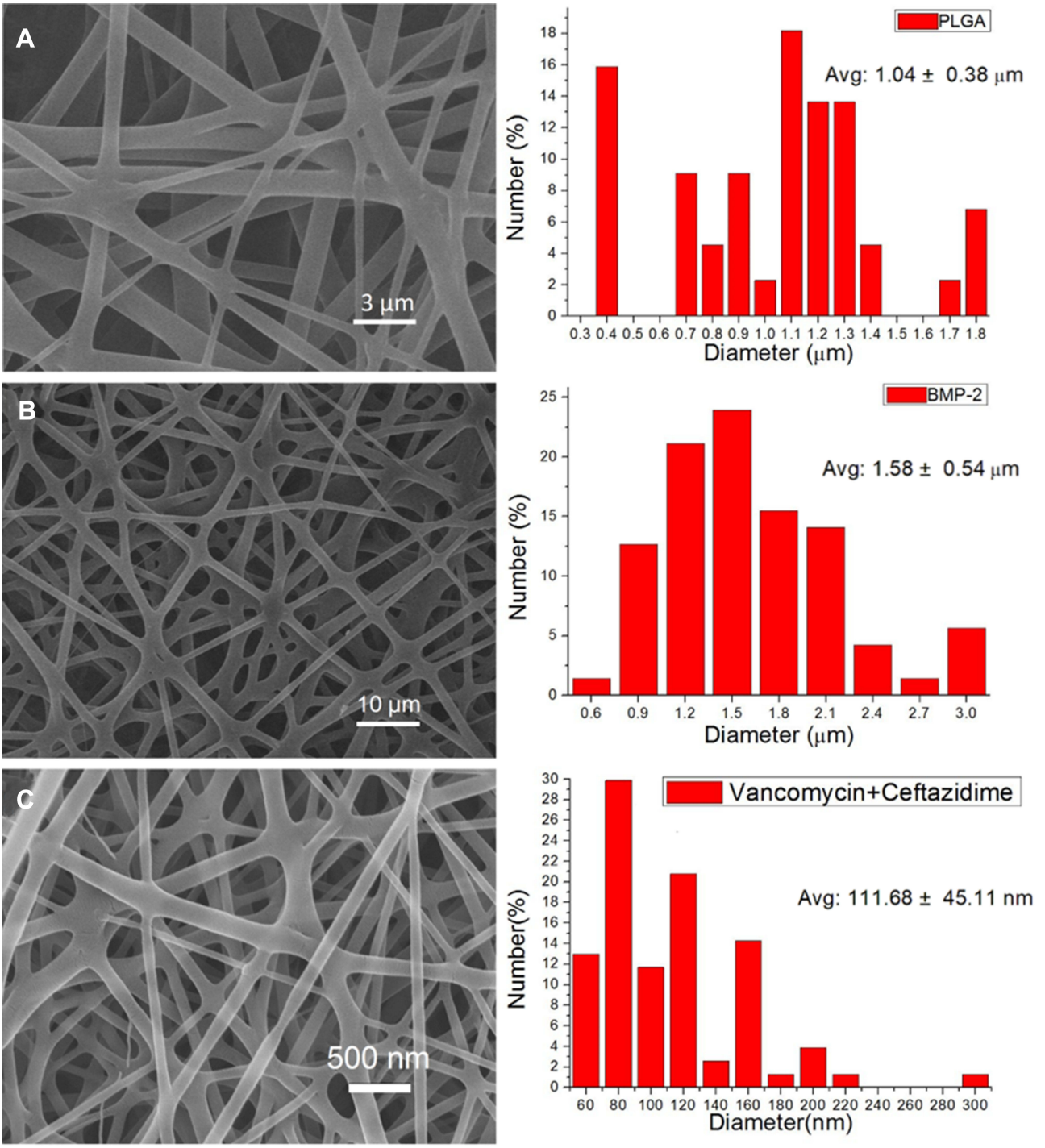

Figure 2 SEM image and fiber diameter distribution of (**A**) pure PLGA nanofibers, (**B**) sheath-core PLGA/BMP-2 nanofibers, and (**C**) PLGA/vancomycin/ceftazidime nanofibers.

trend, revealing a sudden burst release of drug on the first day, followed by a decrease in the concentration on day 7 and a gradual increase in drug release until day 28; the amount of drug released was then maintained until day 42. Throughout the study period, the concentrations of the two antibiotics remained much higher than the minimal inhibitory concentration of 90% (MIC90, 2 μg/mL).[11]

The elution profile of BMP-2 obtained from muscular tissue (Figure 5F) showed a release trend similar to that of the antibiotics, providing a sustainable level for up to 42 days.

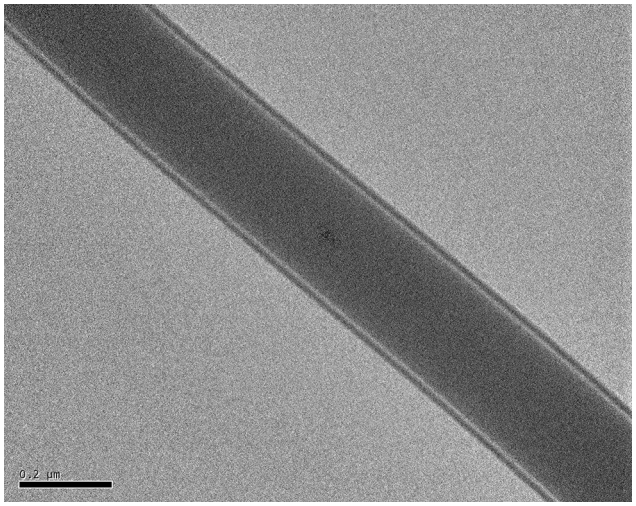

Figure 3 Transmission electron microscopy image of sheath-core nanofibers.

Systemic Blood Examination for Vancomycin/Ceftazidime

Systemic accumulated antibiotic concentrations were also examined from peripheral blood from the studied rabbits. Notably, the concentrations of antibiotics in all samples were lower than the detection limit.

Gross Specimen Examinations

All rabbits were sacrificed at week 8. The target femurs with surrounding muscle tissue were dissected and excised from adjacent anatomical joints (Figure 6A). On examination, the PCL remained intact, and the PLGA nanofibrous membranes were degraded completely. Between PCL mesh and muscular tissue, there was a thick tissue, which we designated the bioactive induced membrane. The cortical continuity of the femur was observed, and the bone defect was filled with a newly formed callus.

Histologic Evaluation

The surfaces of the capsular membranes in both groups were lined by one to three layers of round to spindle cells (Figure 6B). The cells lacked an underlying basement membrane. The deeper layers of the membranes consisted of fibroblast-like spindle cells. Membranous tissue was rich in small blood vessels. Scattered eosinophils and lymphocytes were noted in most cases.

Radiographic Examinations

Figure 6C–E shows the radiographic examination results. The femoral specimens in the PCL group (Figure 6C) showed poor callus formation around the osteotomized site. In addition, the PCL-PLGA/antibiotics/BMP-2 group (Figure 6D) showed better union status than the PCL-PLGA/antibiotics group (Figure 6E).

IHC Analysis

All investigated factors of the induced membrane revealed variable positive staining (Figure 7). The membrane-lining and spindle cells showed diffuse and strong cytoplasmic expression of BMP-2 and TGF-β (Figure 7A and B). vWF was expressed superficially and intensely, whereas VEGF was expressed with similar intensity, but was located deeper than vWF (Figure 7C and D). IL-6 also showed strong expression in the deeper layer (Figure 7E).

Mechanical Properties

The results of mechanical torsional tests are shown in Figure 8. The test femurs in the PCL group possessed the weakest resistance to torsional force, whereas the femurs in the PCL-PLGA/antibiotic and PCL-PLGA/antibiotic/BMP-2 groups exhibited nearly equal torsional strengths similar to that of the healthy femur. There were

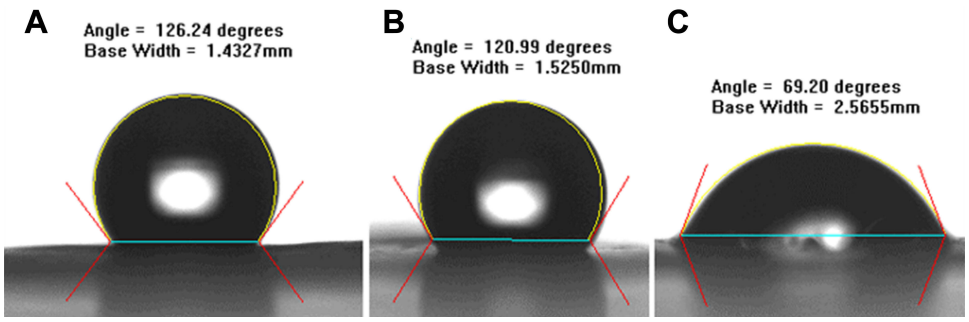

Figure 4 Water contact angles of (**A**) pure PLGA nanofibers (126.24 ± 10.26°), (**B**) sheath-core PLGA/BMP-2 nanofibers (120.00 ± 8.67°), and (**C**) PLGA/vancomycin/ceftazidime nanofibers (69.2.33 ± 5.14°). Substantially improved hydrophilicity of electrospun nanofibers was observed with the addition of water-soluble antibiotics.

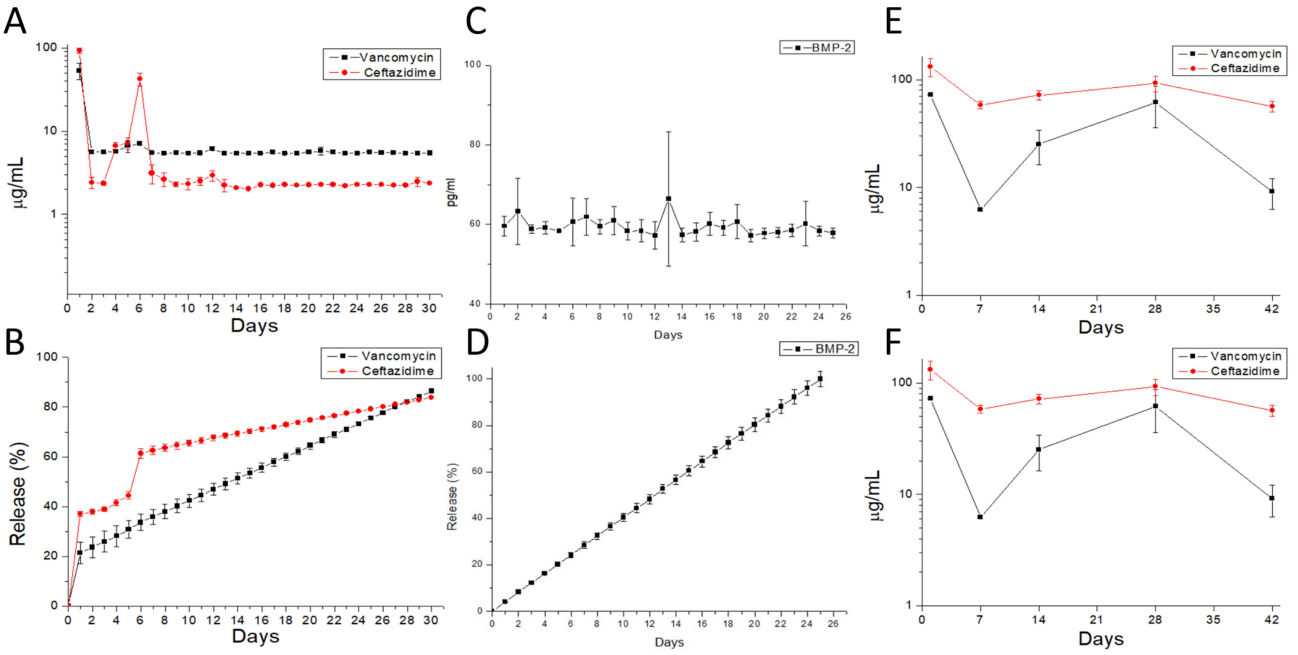

Figure 5 In vitro drug release profiles. (**A**) Daily and (**B**) accumulated release of antibiotics from the composite nanofibers. (**C**) Daily and (**D**) accumulated release of BMP-2 from the composite nanofibers. In vivo examination of the daily release of (**E**) antibiotics and (**F**) BMP-2 from the composite scaffold in the muscular tissue.

no significant differences in the torsional strengths of the femurs between the PCL-PLGA/antibiotic group and PCL-PLGA/antibiotic/BMP-2 group, although the femurs in the PCL-PLGA/antibiotic group had relatively higher torsional resistance.

Discussion

Resorbable polymers have been applied in medical use for more than three decades. These polymers currently have several applications, including use as drug delivery devices and in tissue engineering. In this study, we exploited the drug-eluting composite scaffolds by integrating different fabrication processes (3D printing and electrospinning) and resorbable polymers (PCL and PLGA) for two specific purposes. First, the 3D-printed PCL mesh acted to keep the artificial bone graft in a contained area, providing an organized scaffold for osteocytes during the bone healing process. Secondly, the applied hybrid electrospun and co-axially electrospun PLGA/vancomycin/ceftazidime/BMP-2 nanofibers demonstrated the sustainable release of antibiotics (infection prevention or control) and BMP-2 (osteoinduction capacity) after induction of the bioactive membrane. Both in vitro and in vivo studies showed similar findings, supporting the use of resorbable composite scaffolds in treating segmental bone defects.

Three-dimensional printing is based on the principle of layered manufacturing, in which materials are overlapped layer by layer.[22] This technology can be used to quickly fabricate components with any complex shape by accurately accumulating material using solid modeling according to a computer-aided design model or computed tomography scan under computer control. Biodegradable scaffolds play important roles as bionic structures in the extracellular matrix; however, compared with traditional scaffold-fabrication methods, 3D printing can manufacture any complex structure with both microscopic pores and macroscopic shapes, thus allowing effective control of the microstructure and physicochemical properties of scaffolds.

We designed the PCL mesh to wrap around the bone defect as a bone reservoir to maintain the bone graft or bone substitute for bony repair. The PCL in mesh form provides several advantages. First, the application of PCL mesh onto the bone defect was simple and enabled the mesh to fit defects with different sizes and lengths. Thus, there was no need to adjust the shape or volume of the applied polymer. Additionally, the applied PCL mesh was easily fixed with simple sutures. When the bone reservoir was designed in the 3D cage form, the fixation was more complex than the suture, requiring additional bone screws or plates for fixation. Finally, the resulting fracture repair was complete. The designed PCL mesh was applied on the bone surface, and fracture repair was accomplished directly by bone-to-bone contact. Once the bone reservoir was designed in a cage form, implantation of the cage took

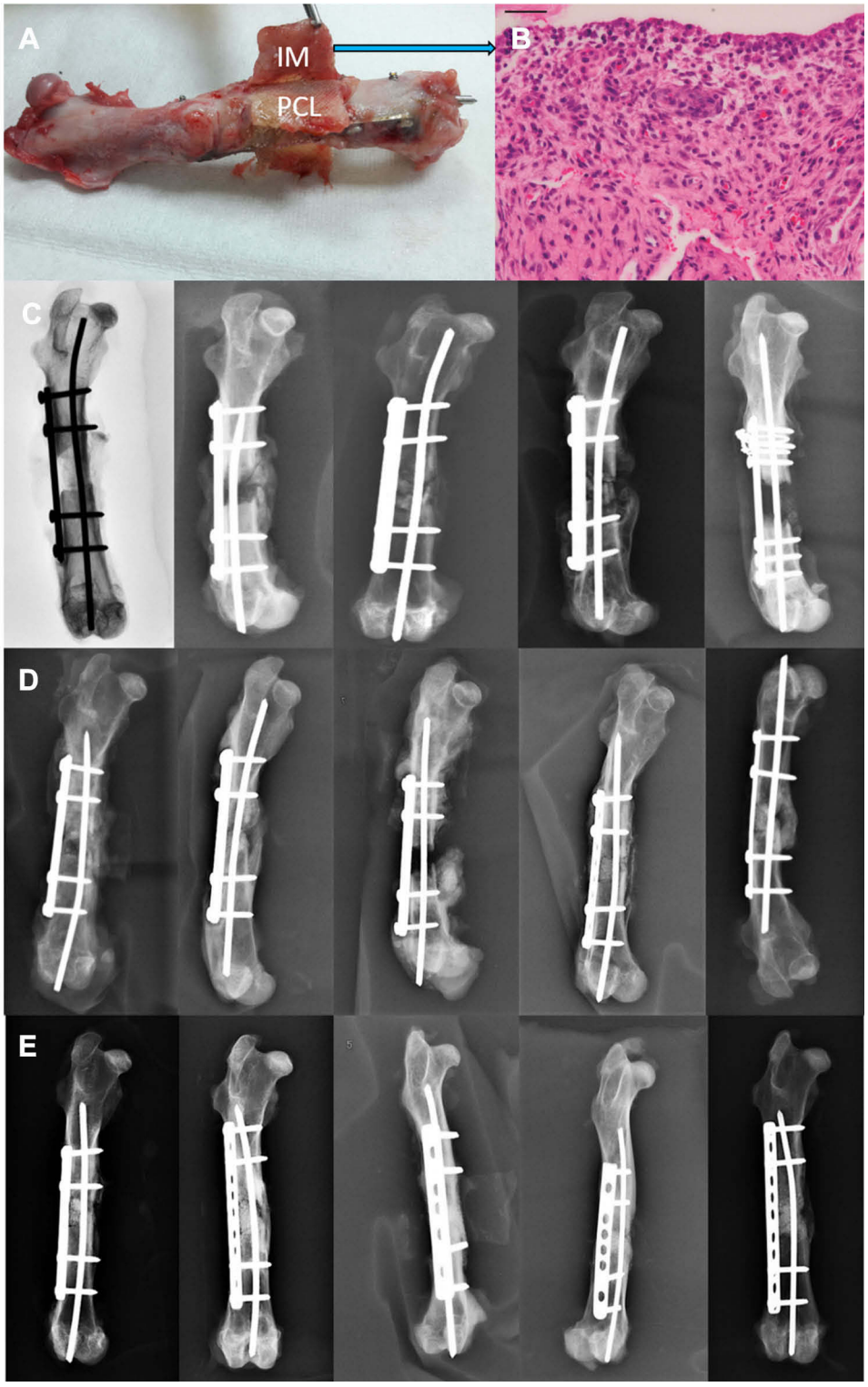

Figure 6 Analysis of the gross specimen (**A**) revealed a thick induced membrane (IM) formed circumferentially around the applied scaffold. The PLGA nanofibers had been dissolved completely, and only the PCL mesh was preserved. The histological evaluation of the induced membrane was performed (blue arrow) and represents in (**B**). (**B**) Histological evaluation by hematoxylin and eosin staining of the induced membrane. Radiographic examination of fracture healing in (**C**) the PCL group, (**D**) the PCL-PLGA /antibiotic group, and (**E**) the PCL-PLGA/antibiotic/BMP-2 group.

up some part of the bony cortex and medulla. Complete fracture repair in rabbits required 3 months and may take even longer in humans. The biodegradation time of PCL is expected to be up to 48 months. Thus, the application of a 3D bone cage on the bone defect may interfere with the fracture healing process.

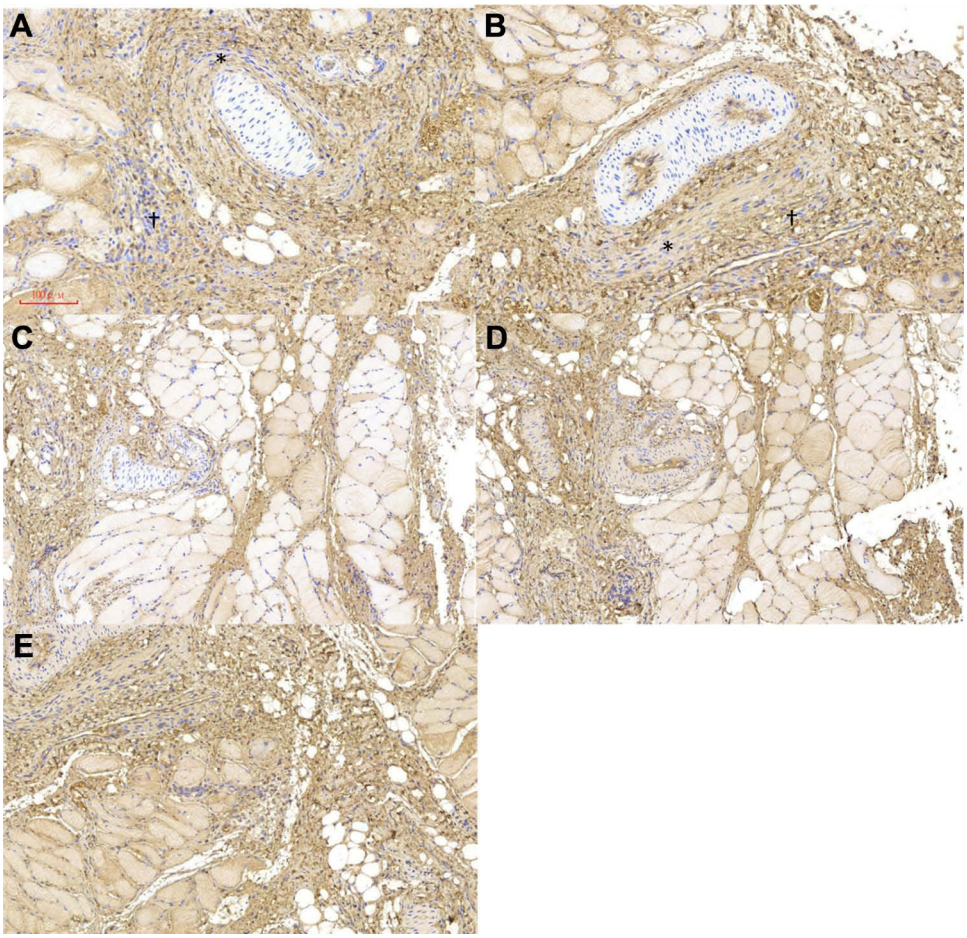

Figure 7 Immunohistochemical analysis of the expression of (**A**) BMP-2 (*membrane-lining cells, †spindle cells), (**B**) TGF-β (*membrane-lining cells, †spindle cells), (**C**) vWF, (**D**) VEGF, and (**E**) IL-6.

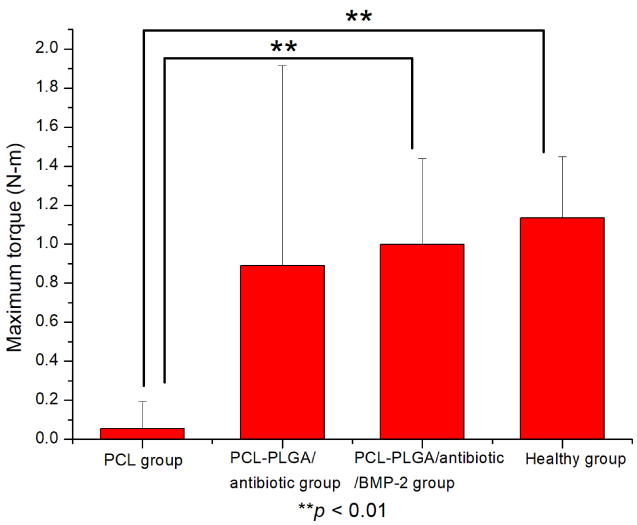

Figure 8 Maximum torques of healed bone in the Masquelet procedure.

In contrast, co-axial electrospinning provides the advantage of realizing the transformation of nanofibers from a single component to complex multilevel structures.[23,24] In addition, core-shell-structured nanofibers can preserve unstable biological reagents or viruses effectively, prevent the decomposition of unstable compounds, and act as materials for the slow release of drugs. Typical applications of co-axially electrospun nanofibers include drug release, encapsulation of different biologically active compounds, cell scaffolds, formation of nanotubes, and nanofluidics. The experimental results also suggested that the overall size of the nanofibers diminished with the introduction of antibiotics. The presence of drugs decreased the content of polymeric material in the nanofibers. The fibers thus possessed less strength to resist the stretching force by the applied electrical forces. The sizes of the electrospun nanofibers reduced accordingly.

The induced membrane technique mainly focuses on treating large bone defects. This technique was first proposed by Masquelet in the 1970s, and several modified procedures have been developed in subsequent years.[25–33] Regarding surgical outcomes following this technique, most studies have shown satisfactory results. However,

there are still two challenges to be overcome. First, whether the environment for new bone formation is infected can affect the failure or success of this practice.[34–36] Second, successful treatment is related to the capacity for bone healing of such large bone defects.[28,29,32]

Antibiotic powder mixed with supplemental bone grafts may be an alternative to control bacterial growth during bone healing.[37–39] However, early depletion of water-soluble antibiotics in an uncontained space limits its bactericidal capacity. Other studies have focused on the implantation of antibiotic-loaded PMMA spacers during the stage one induced membrane technique.[40–42] The ability to halt bacterial growth was sufficient; however, the PMMA spacer still had to be removed surgically in stage two of the induced membrane procedure. The results from our study revealed that a high antibiotic concentration above MIC90 could be maintained by the PLGA nanofibrous membrane for more than 42 days in vivo. In addition, the systemic antibiotic concentration remained low, thus minimizing the possible side effects of systemic toxicity.

The other issue that may cause the failure of the induced membrane technique is the volume of the autograft. Masquelet proposed that the ratio of the cancellous bone allograft to the autograft should not exceed 1/3 because allograft does not contain stem cells or growth factors.[26] However, regardless of the ratio, morbidities and complications from autologous bone grafts from the iliac crest or autogenous bone grafts from a reamer-irrigator-aspirator device have still been observed.[43] The osteoconduction effect of artificial bone substitutes has been studied extensively. The results of this study further demonstrated that with the combined use of high-concentration BMP-2, artificial bone substitutes can exhibit osteoinduction properties, thus providing the advantages of enhanced bone healing while avoiding the potential complications of autografting. In addition, a higher concentration of BMP-2 was detected than the implanted dose, demonstrating that a bioactive membrane was induced from our implanted resorbable drug-eluting scaffolds, and the induced membrane was rich in growth factors, including BMP-2.

Despite the success of our preliminary results, there were some limitations to this study. First, the bone defect model was not an infective bone defect model, and the antibacterial effects of the model were assumed based on the detection of local antibiotic concentrations. However, from the study results, the local concentration of antibiotics was greater than the MIC90 (2 μg/mL), and the bactericidal effects could thus be inferred. Second, although the bone union was satisfactory, the healing process for large bone defects, particularly after traumatic bone loss, in humans may be more complicated than the controlled bone loss in the current study. However, our findings demonstrated that constant release of supplemental BMP-2 occurred from the implanted PLGA nanofibers, providing the bone defect with an important osteoinductive protein during bone healing. Third, we used a noninfected animal model, and it is still unclear whether the antibiotic-loaded nanofibers could perform differently in the context of infection. Further studies of PLGA/antibiotic nanofibers in an infection model are necessary in order to answer this question.

In this study, we developed an effective modified Masquelet procedure for treating segmental bone defects using a 3D-printed PCL scaffold combined with co-axially electrospun PLGA/vancomycin/ceftazidime/BMP-2 nanofibers in a rabbit femoral critical bone defect model. The proposed procedure was found to provide high, sustainable concentrations of antibiotics and BMP-2, thus facilitating bone healing. These results may have applications in the clinical setting; however, additional studies are required to realize the application of this approach for the treatment of large bone defects in humans.

Acknowledgments

The authors would like to thank the Ministry of Science and Technology, Taiwan (contract no. 107-2221-E-182-017) and the Chang Gung Memorial Hospital (contract no. CMRP D2H0032, and CMRPG3H1121) for financially supporting this study.

Disclosure

The authors report no conflicts of interest in this work.

References

1. Oh CW, Apivatthakakul T, Oh JK, et al. Bone transport with an external fixator and a locking plate for segmental tibial defects. *Bone Joint J*. 2013;95-B(12):1667–1672. doi:10.1302/0301-620X.95B12.31507
2. Rigal S, Merloz P, Nen DL, Mathevon H, Masquelet AC. French Society of Orthopaedic Surgery and Traumatology. Bone transport techniques in posttraumatic bone defects. *Orthop Traumatol Surg Res*. 2012;98(1):103–108. doi:10.1016/j.otsr.2011.11.002
3. Demiralp B, Ege T, Kose O, Yurttas Y, Basbozkurt M. Reconstruction of intercalary bone defects following bone tumor resection with segmental bone transport using an Ilizarov circular external fixator. *J Orthop Sci*. 2014;19(6):1004–1011. doi:10.1007/s00776-014-0632-1

4. Bumbasirevic M, Stevanovic M, Bumbasirevic V, Lesic A, Atkinson HDE. Free vascularised fibular grafts in orthopaedics. *Int Orthop*. 2014;38(6):1277–1282. doi:10.1007/s00264-014-2281-6
5. Molina CS, Stinner DJ, Obremskey WT. Treatment of traumatic segmental long-bone defects. A critical analysis review. *J Bone Joint Surg Rev*. 2014;2(4).
6. Morelli I, Drago L, George DA, Galazzi E, Scarponi S, Romano CL. Masquelet technique: myth or reality? A systematic review and meta-analysis. *Injury*. 2016;47 Supple 6:S68–S76. doi:10.1016/S0020-1383(16)30842-7
7. El-Alfy BS, Ali AM. Management of segmental skeletal defects by the induced membrane technique. *Indian J Orthop*. 2015;49(6):643–648. doi:10.4103/0019-5413.168757
8. Gupta G, Ahmad S, Mohd Z, Khan AH, Sherwani MK, Khan AQ. Management of traumatic tibial diaphyseal bone defect by "induced-membrane technique". *Indian J Orthop*. 2016;50(3):290–296. doi:10.4103/0019-5413.181780
9. Uhthoff HK, Poitras P, Backman DS. Internal plate fixation of fractures: short history and recent developments. *J Orthop Sci*. 2006;11(2):118–126. doi:10.1007/s00776-005-0984-7
10. Tseng YY, Liao JY, Chen WA, Kao YC, Liu SJ. Biodegradable poly([D,L]-lactide-co-glycolide) nanofibers for the sustainable delivery of lidocaine into the epidural space after laminectomy. *Nanomedicine (Lond)*. 2014;9(1):77–87. doi:10.2217/nnm.13.42
11. Hsu YH, Chen DW, Tai CD, et al. Biodegradable drug-eluting nanofiber-enveloped implants for sustained release of high bactericidal concentrations of vancomycin and ceftazidime: in vitro and in vivo studies. *Int J Nanomed*. 2014;9:4347–4355. doi:10.2147/IJN.S66526
12. Casagrande S, Tiribuzi R, Cassetti E, et al. Biodegradable composite porous poly(dl-lactide-co-glycolide) scaffold supports mesenchymal stem cell differentiation and calcium phosphate deposition. *Artif Cells Nanomed Biotechnol*. 2018;46(sup1):219–229. doi:10.1080/21691401.2017.1417866
13. Dwivedi C, Pandey H, Pandey AC, et al. In vivo biocompatibility of electrospun biodegradable dual carrier (antibiotic + growth factor) in a mouse model-implications for rapid wound healing. *Pharmaceutics*. 2019;11(4):E180. doi:10.3390/pharmaceutics11040180
14. Kim J, Lima E, Silva R, et al. Anisotropic poly(lactic-co-glycolic acid) microparticles enable sustained release of a peptide for long-term inhibition of ocular neovascularization. *Acta Biomater*. 2019;97:451–460. doi:10.1016/j.actbio.2019.07.054
15. Arabpour Z, Baradaran-Rafii A, Bakhshaiesh NL, et al. Design and characterization of biodegradable multi layered electrospun nanofibers for corneal tissue engineering applications. *J Biomed Mater Res A*. 2019;107(10):2340–2349. doi:10.1002/jbm.a.36742
16. Pan S, Qi Z, Li Q, et al. Graphene oxide-PLGA hybrid nanofibres for the local delivery of IGF-1 and BDNF in spinal cord repair. *Artif Cells Nanomed Biotechnol*. 2019;47(1):651–664. doi:10.1080/21691401.2019.1575843
17. Zolfaghari D, Tebyanian H, Soufdoost RS, et al. Modified PLGA nanofibers as a nerve regenerator with Schwann cells. *Cell Mol Biol (Noisy-Le-Grand)*. 2018;64(14):66–71. doi:10.14715/cmb/2018.64.14.11
18. Kumbar SG, Nukavarapu SP, James R, Nair LS, Laurencin CT. Electrospun poly(lactic acid-co-glycolic acid) scaffolds for skin tissue engineering. *Biomaterials*. 2008;29(30):4100–4107. doi:10.1016/j.biomaterials.2008.06.028
19. Hsu YH, Lin CT, Yu YH, Chou YC, Liu SJ, Chan EC. Dual delivery of active anti-bactericidal agents and bone morphogenetic protein at sustainable high concentrations using biodegradable sheath-core-structured drug-eluting nanofibers. *Int J Nanomed*. 2016;11:3927–3937. doi:10.2147/IJN.S107250
20. Chou YC, Lee D, Chang TM, et al. Development of a three-dimensional (3D) printed biodegradable cage to convert morselized corticocancellous bone chips into a structured cortical bone graft. *Int J Mol Sci*. 2016;17(4):E595. doi:10.3390/ijms17040595
21. Yu YH, Wu RC, Lee D, et al. Artificial membrane induced by novel biodegradable nanofibers in the Masquelet procedure for treatment of segmental bone defects. *J Nanomater*. 2018;2018:8246571. doi:10.1155/2018/8246571
22. Yan Q, Dong H, Su J, et al. A review of 3D printing technology for medical applications. *Engineering*. 2018;4:729–742. doi:10.1016/j.eng.2018.07.021
23. Khaf A, Madihally SV. Recent advances in multiaxial electrospinning for drug delivery. *Euro J Pharm Biopharm*. 2017;112:1–17. doi:10.1016/j.ejpb.2016.11.010
24. McClellan P, Landis WJ. Recent applications of coaxial and emulsion electrospinning methods in the field of tissue engineering. *Biores Open Access*. 2016;5(1):212–227. doi:10.1089/biores.2016.0022
25. Masquelet AC, Fitoussi F, Begue T, Muller GP. Reconstruction of the long bones by the induced membrane and spongy autograft. *Ann Chir Plast Esthet*. 2000;45(3):346–353.
26. Apard T, Bigorre N, Cronier P, Duteille F, Bizot P, Massin PP. Two-stage reconstruction of post-traumatic segmental tibia bone loss with nailing. *Orthop Traumatol Surg Res*. 2010;96(5):):549–553. doi:10.1016/j.otsr.2010.02.010
27. Donegan DJ, Scolaro J, Matuszewski P, Mehta SES. Staged bone grafting following placement of an antibiotic spacer block for the management of segmental long bone defects. *Orthopedics*. 2011;34(11):e730–e735. doi:10.3928/01477447-20110922-16
28. Stafford PR, Norris BL. Reamer-irrigator-aspirator bone graft and bi Masquelet technique for segmental bone defect nonunions: a review of 25 cases. *Injury*. 2010;41(Supple 2):S72–S77. doi:10.1016/S0020-1383(10)70014-0
29. Giannoudis PV, Harwood PJ, Tosounidis T, Kanakaris NK. Restoration of long bone defects treated with the induced membrane technique: protocol and outcomes. *Injury*. 2016;47(Supple 6):S53–S61. doi:10.1016/S0020-1383(16)30840-3
30. Ma CH, Chiu YC, Tsai KL, Tu YK, Yen CY, Wu CH. Masquelet technique with external locking plate for recalcitrant distal tibial nonunion. *Injury*. 2017;48(12):2847–2852. doi:10.1016/j.injury.2017.10.037
31. Cho JW, Kim J, Cho WT, et al. Circumferential bone grafting around an absorbable gelatin sponge core reduced the amount of grafted bone in the induced membrane technique for critical-size defects of long bones. *Injury*. 2017;48(10):2292–2305.
32. Sasaki G, Watanabe Y, Miyamoto W, et al. Induced membrane technique using beta-tricalcium phosphate for reconstruction of femoral and tibial segmental bone loss due to infection: technical tips and preliminary clinical results. *Int Orthop*. 2018;42(1):17–24. doi:10.1007/s00264-017-3503-5
33. Masquelet AC. Induced membrane technique: pearls and pitfalls. *J Orthop Trauma*. 2017;31(Supple5):S36–S38. doi:10.1097/BOT.0000000000000979
34. Giotikas D, Tarazi N, Spalding L, Nabergoj M, Krkovic M. Results of the induced membrane technique in the management of traumatic bone loss in the lower limb: a cohort study. *J Orthop Trauma*. 2019;33(3):131–136. doi:10.1097/BOT.0000000000001384
35. Stella M, Santolini E, Autuori A, Felli L, Santolini F. Masquelet technique to treat a septic nonunion after nailing of a femoral open fracture. *Injury*. 2018;49(Supple4):S29–S33. doi:10.1016/j.injury.2018.11.017
36. Morris R, Hossain M, Evans A, Pallister I. Induced membrane technique for treating tibial defects gives mixed results. *Bone Joint J*. 2017;99-B(5):680–685. doi:10.1302/0301-620X.99B5.BJJ-2016-0694.R2
37. Chan YS, Ueng SW, Wang CJ, Lee SS, Chao EK, Shin CH. Management of small infected tibial defects with antibiotic-impregnated autogenic cancellous bone grafting. *J Trauma*. 1998;45(4):758–764. doi:10.1097/00005373-199810000-00023
38. Shiels SM, Raut VP, Patterson PB, Barnes BR, Wenke JC. Antibiotic-loaded bone graft for reduction of surgical site infection in spinal fusion. *Spine J*. 2017;17(12):1917–1925. doi:10.1016/j.spinee.2017.06.039

39. Kanakeshwar RB, Jayaramaraju D, Agraharam D, Rajasekaran S. Management of resistant distal femur non-unions with allograft strut and autografts combined with osteosynthesis in a series of 22 patients. *Injury*. 2017;48(Suppl2):S14–S17. doi:10.1016/S0020-1383(17)30488-6
40. Nau C, Seebach C, Trumm A, et al. Alteration of Masquelet's induced membrane characteristics by different kinds of antibiotic enriched bone cement in a critical size defect model in the rat's femur. *Injury*. 2016;47(2):325–334. doi:10.1016/j.injury.2015.10.079
41. Shah SR, Smith BT, Tatara AM, et al. Effects of local antibiotic delivery from porous space maintainers on infection clearance and induction of an osteogenic membrane in an infected bone defect. *Tissue Eng Part A*. 2017;23(3–4):91–100. doi:10.1089/ten.tea.2016.0389
42. Luangphakdy V, Elizabeth Pluhar G, Piuzzi NS, et al. The effect of surgical technique and spacer texture on bone regeneration: a caprine study using the Masquelet technique. *Clin Orthop Relat Res*. 2017;475(10):2575–2585. doi:10.1007/s11999-017-5420-8
43. Dimitriou R, Mataliotakis GI, Angoules AG, Kanakaris NK, Giannoudis PV. Complications following autologous bone graft harvesting from the iliac crest and using the RIA: a systematic review. *Injury*. 2011;42(Suppl2):S3–S15. doi:10.1016/j.injury.2011.06.015